Journal of Power Sources 198 (2012) 368–377

Contents lists available at SciVerse ScienceDirect

Journal of Power Sources

journal homepage: www.elsevier.com/locate/jpowsour

Modeling and optimization of a hybrid power system for an unmanned surface vehicle

Neeta Khare*, Pritpal Singh[1]

Department of Electrical and Computer Engg., Villanova University, 800E, Lancaster Ave, Villanova, PA, 19085, USA

ARTICLE INFO

Article history:
Received 19 August 2011
Received in revised form
22 September 2011
Accepted 23 September 2011
Available online 1 October 2011

Keywords:
Hybrid power system
Unmanned surface vehicle
Hybrid power system optimization
Nonlinear optimization

ABSTRACT

Modeling and optimization of a hybrid power system comprising several different power sources provides a tool to size the individual power system components and to optimize the power system control variables. The hybrid power system is required to meet the demanding requirements of long duration mission of unmanned surface vehicles (USVs). These demands for power may be met by a combination of renewable energy resources, conventional fossil-fueled energy sources and energy storage options. The hybrid power system being considered here comprises a solar array, an ocean wave energy converter, a fuel cell system, a diesel generator and a lithium ion battery pack. The approach gives high priority to natural energy sources, i.e. solar and wave energy converter within the discrete time domain followed by minimization of a cost/energy ratio associated with the storage based energy elements, i.e., battery pack, fuel cell system (H_2 storage) and diesel generator (fuel storage). The results show that optimization has been achieved with 19.6% contribution by solar power during daylight hours and 5.53% contribution of the wave energy harvester to meet the load demands. The battery bank contributes 39.7% which is 4.4% above the fuel cell contribution. The diesel generator does not contribute during the stealth mode of operation of the USV mission. The average percentage energy contribution from each source confirmed the priorities based on minimization of cost/energy ratio of hybrid power elements. However, in the first case study the optimized result shows a constraint violation when fuel cell performs slightly higher than the battery. Later, in the second case study, it is corrected by increasing the size of the battery bank.

1. Introduction

Hybrid power system management is an ongoing research area to provide a reliable power solution to electric vehicles (EV)/hybrid electric vehicles (HEV). This paper focuses on the problem of optimized hybrid power management to meet the needs of an unmanned surface vehicle (USV). The USV, an 11 m Rigid Hull Inflatable Boat (RHIB) platform is expected to conduct Intelligence, Surveillance and Reconnaissance (ISR) missions in the sea for up to two weeks duration. An USV design methodology is explored for a unique hybrid power system. For the present work, the hybrid power system includes the following power sources:

- solar panels,
- wave energy harvester,
- battery bank,
- fuel cell system, and
- diesel generator.

In previous work, Villanova's research group has performed the sizing analysis, weight analysis, modeling and characterization of each power source for an USV hybrid power system [1–3]. Narayan and Singh [1] explored the types of battery and fuel cell that could be used in the Rigid Hull Inflatable Boat (RHIB) platform for USV. The authors worked on preliminary characterization and analysis of the Li-ion battery and fuel cell. They developed a Simulink® model of the battery and the fuel cell. Ramachandrudu and Singh [2] developed a prototype for wave energy conversion using an octagonal linear generator (OLG). The authors modeled a prototype using the computer aided design (CAD) software tool SolidWorks© before physical design implementation. A prototype capable of producing an output voltage of 0.21 V and an output current of 2.3 mA was fabricated. The results were validated using a numerical algorithm model implemented in Matlab/Simulink environment, for a wave frequency of 4 Hz and a wave velocity of 0.18 m s^{-1}. The Simulink model was later used to develop a scaled modeled for the USV. Knauff et al. [3] developed and implemented an equivalent electric circuit model of a Li-ion battery in the Matlab/Simulink

* Corresponding author. Tel.: +1 610 599 6134.
E-mail addresses: Neeta.khare@villanova.edu (N. Khare), Pritpal.singh@villanova.edu (P. Singh).
[1] Tel.: +1 610 519 7378; fax: +1 610 519 4436.

0378-7753/$ – see front matter © 2011 Elsevier B.V. All rights reserved.
doi:10.1016/j.jpowsour.2011.09.080

environment. To develop a circuit model, the authors experimented with a charging/discharging cycles of a battery. Later the state of charge (SOC) of a battery was shown as a function of the circuit components. The present work is an extension of previously studied power sources, in a unique framework to provide an optimized solution for the design of a hybrid power system for an USV to perform ISR operations.

Normally, the optimization of a hybrid power system is difficult to converge to a unique solution because the objective function includes nonlinear modeling of each power source and each model term comprises large power control variables, i.e., solar irradiation, solar panel current and voltage, number of solar panels, battery discharge current, battery discharge time, battery state of charge, H_2 flow rate, H_2 pressure, sea wave oscillation, wave energy conversion factor, diesel generator conversion factor, fuel storage capacity, fuel consumption rate, etc. Fellow researchers have worked on hybrid power system controller design and optimization using various methodologies for the hybrid power plants or for electric vehicles (EV). Uzunoglu et al. worked on modeling, controlling and simulating a hybrid system consisting of a photovoltaic (PV), fuel cell (FC) and ultra capacitor (UC) systems for sustained power generation [4]. In the simulation model, the PV system feeds an electrolyzer to produce hydrogen for future use. If the PV system output is not sufficient to meet the load demands, the FC system takes over to meet the remaining load. If the load demand increases further beyond the FC capacity, an UC bank meets the load demand. This is a simple hierarchical-based controller design to address the hybrid system control.

A three layer intelligent hybrid power management strategy was developed by Hajizadeh et al. [5]. The authors described a hierarchical hybrid controller between dual energy sources consisting of a battery bank and a solid oxide fuel cell (SOFC) system. The method uses a supervisory control layer for decision making, a fuzzy logic layer for splitting power between the battery and fuel cell and a third and final layer for a local controller to regulate the set points.

Jeong et al. also worked on a fuzzy logic-based energy management approach for a hybrid power system [6]. This simple strategy uses if-then rules to manage energy from a battery and a fuel cell. All three papers described above have used simple hierarchical-based control design and did not look for an economic solution for the system design.

A unique stochastic optimization approach has been used by Moura et al. for a plug-in hybrid electric vehicle (PHEV) [7]. The paper focuses on optimizing PHEV power management for fuel economy over the battery energy saving in an individual drive cycle using stochastic dynamic programming.

The following two research papers have used the energy hub concept to optimize the hybrid system problem. The energy hub allows the interfacing or coupling between energy demand and energy supply. Fabrizio et al. worked on optimizing multi energy systems in building design [8]. The authors used cost optimization on the energy converters and on the energy storage during the concept state of building design to minimize the initial investment cost. The second paper by del Real et al., describes element sizing in a hybrid power system [9]. The objective function minimization is based on the cost efficiency of the system demands. The hybrid system considered in the paper includes wind generation, batteries and fuel cell power sources.

The hybrid power model has been successfully applied in electric vehicles to meet their challenges of dynamic and unpredictable power requirements. Moreover, the optimized hybrid power system design can provide reliable vehicle operation and sustainability. Also, solar energy, wave energy, battery and fuel cell sources can save the environment from the harmful impact of conventional fuel consumption.

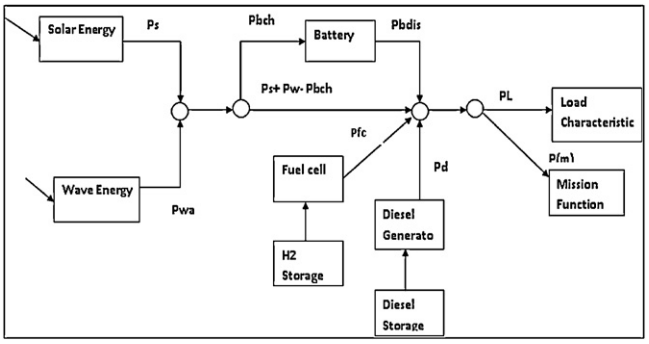

Fig. 1. Basic framework for power optimization. Solar array power, P_s; wave power, P_{wa}; fuel cell system output, Pfc; diesel generator, P_d; battery charging characteristic, P_{bch}, battery discharging characteristic.

In the present study, the hybrid power system is a combination of natural energy sources (sun and wave) and energy sources based on storage (battery bank, fuel cell and diesel generator). When these natural energy sources are available, they should be used at their maximum capacity and are preferred over the other energy sources. The cost optimization as used in the previous research, if applied, would result in underutilizing available energy from sun and wave. On the other hand, hierarchical approach described in previous papers could not provide an economic design for a hybrid system because it would use a fixed hierarchy of the power sources. The fixed hierarchy would not prioritize the power sources to achieve a cost effective solution by making the cost/energy ratio minimum for a generic design of a hybrid power system. Therefore, the present paper contributes by developing a unique simplified solution based on modular optimization. The approach uses two modules (1) prioritizing based on availability and (2) cost consumption optimization. The solar array power and wave power sources are prioritized based on their availability during the day and night and the cost optimization is applied to the remaining sources so as to minimize the cost/energy ratio. The discrete time optimization is applied on the objective function which is defined as an error between the energy demand and energy supply. The prioritization of sources based on their availability and the cost optimization prevent a system from over sizing because the natural resources are utilized fully and the other energy resources provide the smaller balance of energy required. Optimized results provide a reasonable/judicious size of the storage based energy sources so as to prevent an undersized system design at crucial load demand at any discrete time of operation.

The framework for optimizing the USV power system in Fig. 1 shows a hybrid power system arrangement with five power sources and an USV load profile. The solar array and wave harvester directly feed to the USV load on the availability of sun and wave. The control variables, constraints and bounds are set to use solar and wave energy to their maximum limit and minimize the use of other more expensive power sources. Solar power (or wave power) charges the battery when the supply is higher than the demand. The other three energy sources, i.e., battery bank, fuel cell system and diesel generator contribute to the load demand if solar energy and wave energy output are not sufficient.

The cost minimization is applied on the storage energy sources, i.e., battery bank, fuel cell system and diesel generator. Solar power is described as a function of solar irradiation and time of day whereas wave power generator output is modeled using the oscillation of the wave and a power conversion factor for the linear generator. The fuel cell system output is considered here as a function of hydrogen pressure and hydrogen flow rate. The diesel generator output is a function of fuel consumption per hour. The

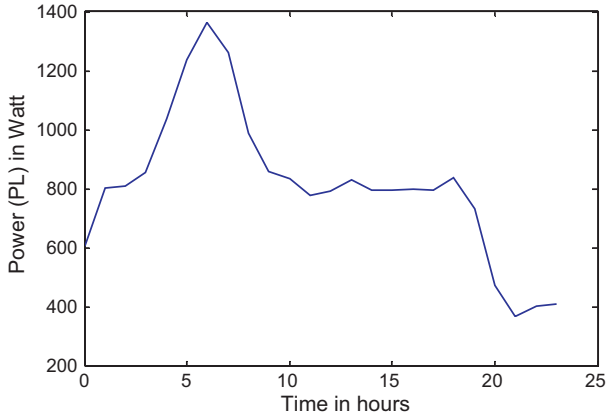

Fig. 2. Load profile (PL) of USV within 24 h.

battery model depends on the charging or the discharging current and the battery terminal voltage.

2. Load profile and mission for USV

The USV is expected to conduct an ISR mission relying on power supplied by a unique hybrid system. The hybrid power system employs a diesel generator, lithium-ion battery pack, fuel cell system, wave power and a solar array. Currently, the assumed speed requires the USV to begin by running on diesel power for 3 h at 45 knots from a mother ship to the area of deployment. It then switches over to the hybrid scheme and runs for 336 h at 5 knots while performing surveillance in stealth mode. Finally it returns to the mother ship on diesel power running at 45 knots for 3 h [10]. Every aspect of the hybrid power system for this mission must be closely analyzed and properly sized if the USV is to accommodate the resources for accomplishing a mission of such long duration. The stealth mode for the Maritime Security (MS) mission define with the activities such as strategic and tactical intelligence collection, chemical, biological, nuclear, radiological, explosive detection and localization, near-land and harbor monitoring, deployment of leave-behind surveillance sensors, and specialized mapping object, detection, localization.

The expected load profile of the USV needed to support the MS mission objective is shown in Fig. 2.

The MS load profile for stealth operation consists of a static demand (PL) as shown in Fig. 2 and a random demand (P_m) as shown in Fig. 3. PL profile describes an initial high power requirement for propulsion to achieve a constant speed of the boat. This peak signal is followed by a constant power demand to power up the payloads

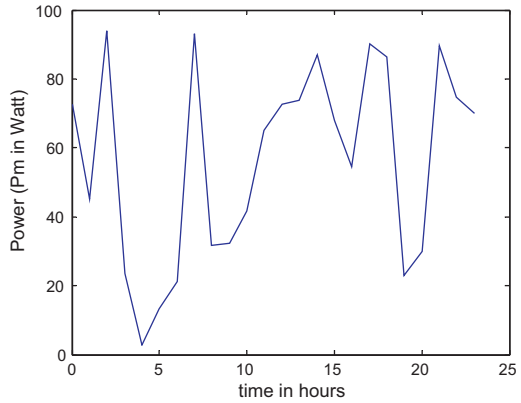

Fig. 3. Random power demand P_m for USV operation.

to perform ISR operations during the mission and further reduced to a lower value to run just mandatory load for smooth sailing of the USV vehicle. The PL load profile is modeled as the sum of sinusoidal signals and is given by Eq. (1) and is shown in Fig. 2:

$$\mathrm{PL} = f\{\sum(a\sin(bt + c))\} \tag{1}$$

where a, b and c are constants and t is time.

The mission objective also includes some random power (P_m) requirement to accommodate sudden actions needed for security such as generation of acoustic signals, magnetic signals, and pressure signals for an object detection and to operate lethal payload (deck gun). A uniform pseudorandom number generator algorithm in Matlab is used to generate the random number streams shown in Fig. 3. The streams are independently generated each time the algorithm is executed.

The load profile (PL) and random power demand (P_m) determine the total power requirement for the USV on the hybrid power system during operation.

The goal of our work is to optimally match the power source mix to the mission using the design illustrated in Fig. 1. The constraint that applies to the total power flow to limit the load profile in the system is given by Eq. (2).

$$\underline{\min P_i} \le P_i^t \le \overline{\max P_i} \quad \forall t, \quad \forall i \tag{2}$$

where i is an index representing a particular power source subsystem to be optimized, t is time, $\underline{\min P_i}$, and $\overline{\max P_i}$ represent the lower and the upper bounds of power flow in the system. These maximum and minimum values of power flow can be varied with speed profile, class of fleet and mission objectives.

While the USV mission is planned for 14 days duration, the present paper describes modeling of the first 24 h of the total of 336 h period. To extend the model for 14 days (336 h), we need to understand the load profile in detail. In the beginning of the stealth portion of the mission the boat requires an initial high power for propulsion to achieve a speed of 5 knots and later reduces to a lower value to accommodate mandatory load and random power requirements for sudden actions needed for security. During the stealth mode of operation, the boat needs to maintain a constant speed to perform ISR operations. In Fig. 2, the first 10 h of load profile are for propulsion and represent a transient period. The next 14 h (in Fig. 2) show the stealth mode. In ideal conditions, the load profile will repeat the latter pattern during the rest of the period (326 h). Assuming ideal conditions, we have decided to limit the current scope of the work to 24 h. Moreover, we are working on a 336 h optimization model.

3. Modeling of power sources

3.1. Solar array power

The USV master plan [10] suggests using an 11 m RHIB for ISR operations (MS mission). Fifteen nominally 200 W solar panels conveniently fit onto the 11 m vessel. The solar panel output power P_s is modeled using experimental data shown in Figs. 4–6. Solar power is seen as a function of solar radiation intensity (G) and time (t) [11].

Fig. 4 shows a power fit on the experimental data of solar array power and solar intensity range from 700 W m^{-2} to 1000 W m^{-2} collected in Philadelphia during the month of April 2009 using south facing panel at 60° angle. The power fit is preferred for this study as given by Eq. (3):

$$P_s(G) = aG^b \tag{3}$$

where $a = 1.501e^{-0.05}$ and $b = 2.213$ are constants.

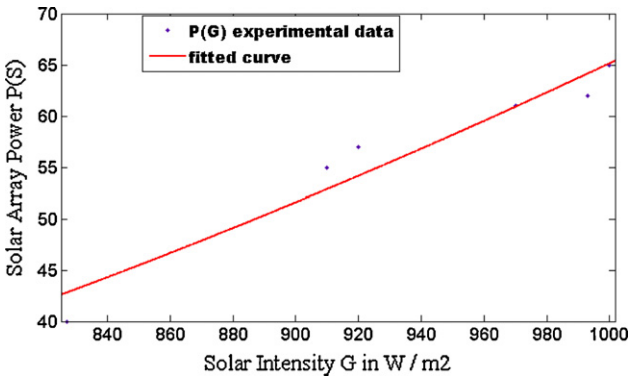

Fig. 4. Solar power (P_s) in W vs. solar intensity (G) in W m^{-2}.

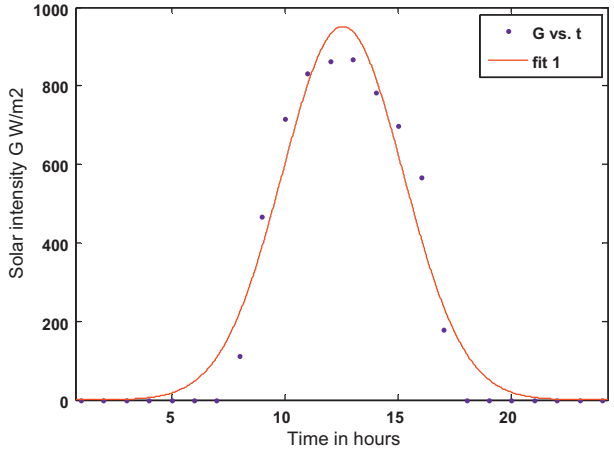

Fig. 5. Solar intensity (G) vs time (t).

The power curve demonstrates a fit with a fitness result of sum of squares error (SSE) is 17.8, R-square is 0.9182 and coefficients are with 95% confidence bounds.

Fig. 5 shows solar intensity vs. time (0–24 h) relation based on the National Solar Radiation database [12]. The general model Gaussian fit, shown in Eq. (4)

$$G(t) = a1\, e^{-((t-b1)/c1)^2} \tag{4}$$

where $a1$, $b1$ and $c1$ are constants.

In Fig. 5, the solar intensity except hours 8–18 is below 100 W m^{-2}. The solar panel can hardly generate any output current

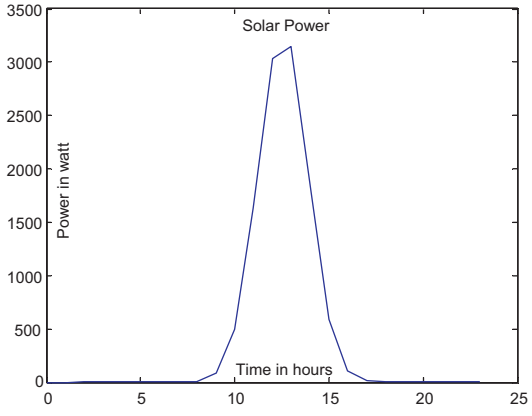

Fig. 6. Solar power (P_s) vs. a day time.

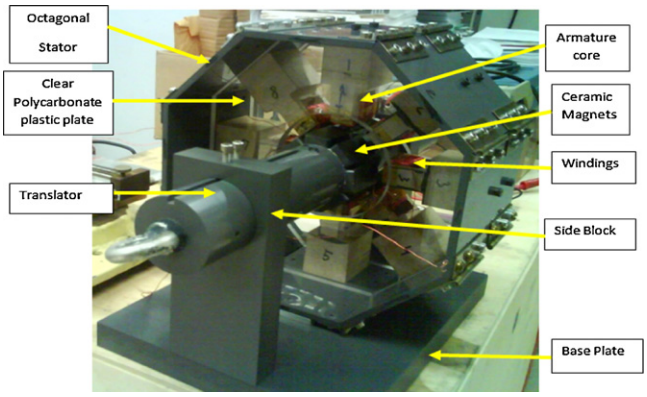

Fig. 7. Octagonal linear generator as power take-off.

with the intensity below 100 W m^{-2}. Therefore, we have considered effective sun light hours of the day from 8.00 am to 6.00 pm.

The fitness result is given as root mean square of error (RMSE): 71 and R-square: 0.9625.

Combining Eqs. (3) and (4) represents solar power for fifteen panels as a function of time shown in Fig. 6 and given by Eq. (5).

$$P_s = a\,(a1\, e^{-((t-b1)/c1^2)^b}) \tag{5}$$

3.2. Wave power

The wave power P^t_{wa} at time t is a function of wave oscillation (F_{wa}) and linear generator conversion factor (C_{wa}) given in Eq. (6):

$$0 \le P^t_{wa} \le [C_{wa}F_{wa}] \tag{6}$$

A numerical model of the octagonal linear generator (OLG) was used for the wave power computation. The model was based on the wave energy conversion (WEC) design of a direct driven permanent magnet buoy [13]. A model of the octagonal permanent magnet linear generator with a translating armature, shown in Fig. 7, is designed to extract the energy from the relative movement of the structure with respect to the incident wave.

The harvester design extracts energy by capturing the oscillating motion of the waves to provide mechanical back and forth input movement to a permanent magnet linear generator shaft. The concepts of the Pelamis wave energy converter and the longitudinal flux linear generator have been adapted to design an octagonal linear generator [14]. The evaluation of the design and performance of the model was done to estimate the capability of the device as an additional power source for a USV.

A linear generator wave power model is described by a set of equations. The electromotive force of one coil for a single phase is given by Eq. (7), current output is given by Eq. (8) and wave power linear generator output is given by Eq. (9).

$$e(t) = 2Nv(t)\{l_s B[x(t)] + 2(l'_s - l_s)B'[x(t)]\} \tag{7}$$

$$\left.\begin{aligned} i(t) &= 1/L_m \int e(t) \\ L_m &= (\mu_0 \pi D_m N^2 l'_s)/2k_s\delta \end{aligned}\right\} \tag{8}$$

where

- l_s is the length of the magnet
- l'_s is the length of one side of the coil
- $v(t)$ is the velocity of sea wave
- $B[x(t)]$ is the flux density along the permanent magnet
- $x(t)$ is the shift of the linear generator translator with respect to the incident wave
- $B'[x(t)]$ is the flux density over the $(l'_s - l_s)$ zone

Table 1
Linear generator scaled up model.

Design specification	Prototype model	Scaled model	Comments
Number of turns in coil	400	800	100% increase
Stator outer length (one side)	2.65 in./0.067 m	7.87 in./0.2 m	Increased by 196%
Stator inner length (one side)	2.44 in./0.06 m	7.08 in./0.18 m	190% increase
Armature core height (one side)	2.05 in./0.05 m	4.1 in./0.104 m	Close to 100% increase
Armature core length (one side) (l'_s)	2.36 in./0.0635 m	5 in./0.127 m	Close to 100% increase
Armature core wire (one side)	50 turn	100 turns	100% increase
Magnet height (one side) (L_s)	0.984 in./0.025 m	1.9 in./0.048 m	93% increase
Number of magnets	8	16	100% increase
Support structure ($H \times L \times W$)	5.09 in. × 2.95 in. × 0.98 in./0.129 m × 0.074 m × 0.024 m	11.81 in. × 2.75 in. × 0.787 in./0.3 m × 0.07 m × 0.02 m	The support block increased by 73.7% in total dimension

- L_m = magnetizing inductance
- μ_0 = permeability of free space = $4\pi \times 10^{-7}$ m kg s^{-2} A^{-2}
- D_m = Mean diameter of the winding
- N = number of turns
- K_s = saturation factor
- δ = air gap

$$P_{wa} = e(t)i(t) \tag{9}$$

Considering the model specifications as $N = 800$, $l'_s = 0.127$ m, $l_s = 0.048$ m, $B[x(t)] = B_{\max} \int [v(t)]$, and $B_{\max} = 0.244$ T, the wave power output P_{wa} is plotted as a function of the frequency shift of the linear generator shaft (translated into the wave frequency) given in Fig. 8. The expected power generated at low frequency (1 m s^{-1}) is approximately 50 W.

The wave power parameters are not included in the optimization because we would like to use the maximum wave power on its availability. The wave power model is limited for an operating range of wave amplitude and angular velocity at 1 m and 0.6π rad s^{-1} [$V_m \sin(2\pi ft)$], respectively to generate a maximum power of 50 W for the present study.

Table 1 shows the prototype and scaled up model specifications. The scaled up model has increased close to 116% in over all dimension when compared to the prototype. The estimated mass of the wave energy generator model is approximately 26 kg using a power:weight ratio given in Ref. [14]. This expected mass is 0.3% of the mass of an 11 m USV target vehicle given in the mass analysis in Table 2 [15].

However, the mass of the linear generator will depend on the material used to make the octagonal structure.

Table 2
Mass analysis of USV vessel.

Total system weight		
Boat	7803	kg
H_2 storage module	306	kg unit^{-1}
Fuel cell system	227	kg unit^{-1}
2400 psi canister	116	kg unit^{-1}
Li-ion battery bank	487	kg
Desalination system	32	kg
Deionization system	35	kg
Electrolyzer	25	kg
Solar panel	15	kg unit^{-1}
Total weight	11,494	kg

3.3. Diesel generator

The diesel generator provides the power needed to propel the USV at high speed (45 knots) to and from the mother ship to the deployment area and back to the mother ship. The noisy and costly diesel power is not used during the stealth mode of USV operation. The diesel generator power P_d output given in Eq. (10) is a function of diesel storage capacity D_s and generator conversion factor C_d.

$$0 \le P_d \le [C_d D_s] \tag{10}$$

D_s is measured as diesel consumption in gal h^{-1}, here, upper and lower bounds of the consumption are $2 \le D_s \le 160$. Eq. (11) and Fig. 9 show the P_d based on the statistical data available through diesel services and supply [16].

$$P_d = 25.954e^{0.1809D_s} \tag{11}$$

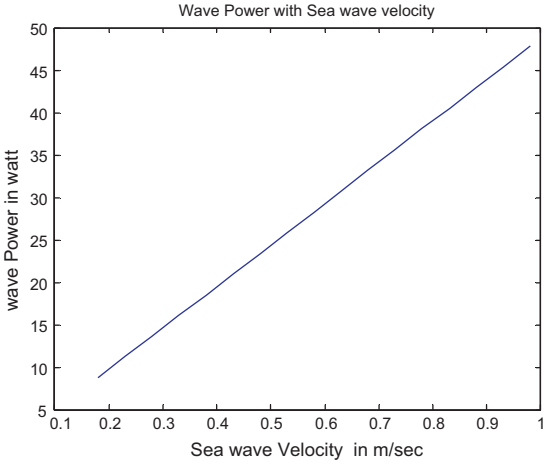

Fig. 8. Wave power output of scaled-up model at fixed wave amplitude.

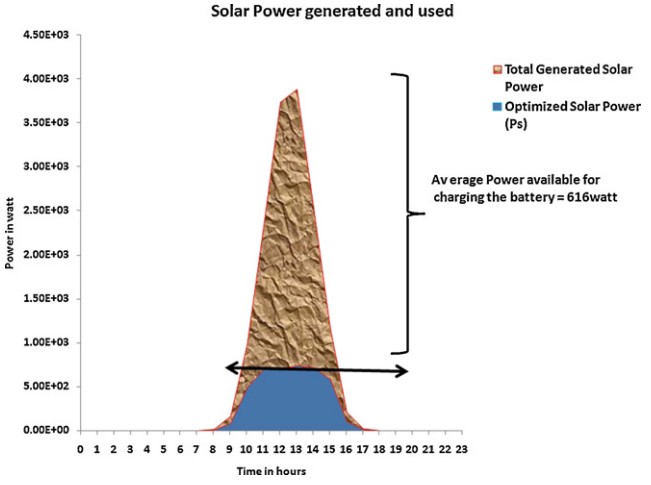

Fig. 9. Diesel power (P_d) vs. diesel consumption.

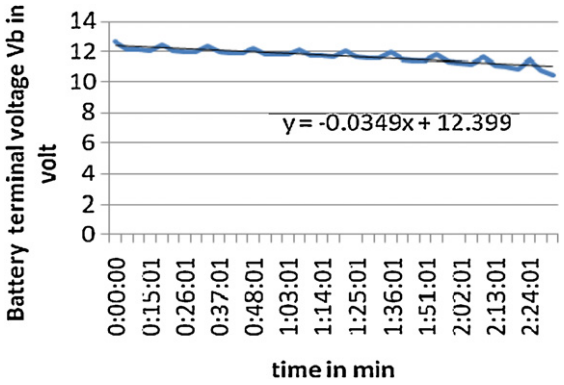

Fig. 10. Battery discharge characteristic.

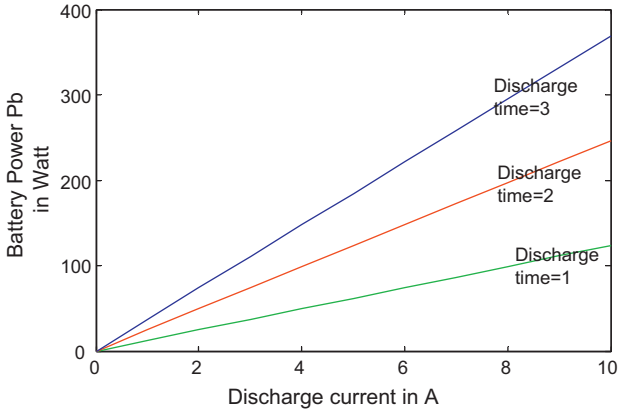

Fig. 11. Battery discharge power as a function of discharge current and discharge time.

3.4. Battery bank

$\bar{E}_B^t$ is energy stored in the battery bank, which should not attain a value more than 93% of its maximum value E_B and should never fall below 20% of the maximum E_B during deep discharge as seen in Eq. (12).

$$0.2 \max \bar{E}_B \le E_B^t \le 0.93 \max \bar{E}_B \tag{12}$$

The battery gets charged whenever the available solar power or the wave power is higher than the load demand. This charging current collects as battery energy if battery energy is less than 93% of maximum E_B.

The collected energy during charging is $E_{B\text{char}} = f(I_{\text{char}}, V_b, t_{\text{char}})$, where I_{char} is charging current, V_b is battery terminal voltage and t_{char} is charging time.

Discharging of the battery is initiated with the optimization module when the solar or the wave power is not sufficient to drive the payload and the battery has more than 20% of its maximum E_B energy. The battery bank supplies the discharge current to meet the remaining power requirement specified by the cost optimization between fuel cell, diesel and battery stored energy. The energy that the battery loses during discharge is given by $E_{B\text{dis}} = f(I_{\text{dischar}}, V_b, t_{\text{dischar}})$, where I_{dischar} is discharging current. To define the battery discharging, an experiment was carried out on a battery string (a series connection of 4 cells each of 3.7 V) to generate the discharge curve shown in Fig. 10. The discharge was conducted for 10 min followed by a rest period of 1 min. The discharge curve shows the small voltage recovery peaks during the rest period. The linear fit on the battery terminal voltage as a function of discharge time is expressed as Eq. (13).

$$V_b = -0.0349 t_{\text{dischar}} + 12.399 \tag{13}$$

The power output of the battery, as a function of discharge current and discharge time, is shown in Eq. (14) and plotted in Fig. 11. The maximum discharge current allowed is 10 A and the maximum discharge duration is 3 h.

$$P_b = I_{\text{dischar}}(-0.0349 t_{\text{dischar}} + 12.399) \tag{14}$$

3.5. Fuel cell

A proton exchange membrane fuel cell (PEMFC) model described in [4] is used in this study. This model is built on the relationship between the output voltage and partial pressure of hydrogen, oxygen and water.

The FC system parameters used in this model are as follows:

N_0, number of series fuel cells in the stack
N_S, number of stacks used in the FC power plant
Ph_2, hydrogen partial pressure [atm]
Ph_2O, water partial pressure [atm]
PO_2, oxygen partial pressure [atm]
qh_2, input molar flow of hydrogen [kmol s^{-1}]
R, universal (Rydberg) gas constant [J $kmol^{-1}$]
T, absolute temperature [K]
U, utilization rate
F, Faraday's constant
Ifc, FC system current [A]

The cell voltage for the PEMFC is obtained from the sum of the Nernst voltage, the activation over-voltage, and the ohmic over-voltage. The activation over voltage and ohmic voltage are ignored for this study. Assuming constant temperature and oxygen concentration, the FC output voltage may be expressed as in Eq. (15) [17,18].

$$V_{\text{cell}} = E + \eta_{\text{act}} + \eta_{\text{ohmic}} \tag{15}$$

The Nernst instantaneous voltage may be expressed by Eq. (16) [17]

$$E = N_0 \left(E_0 + \left(\frac{RT}{2F}\right) \left(\log \left(\frac{10 Ph_2 \left(PO_2^{0.5}\right)}{Ph_2O} \right) \right) \right); \tag{16}$$

The FC system consumes hydrogen according to the power demand. The hydrogen is obtained from the on-board high pressure hydrogen tanks. Depending on the FC system configuration, and the flow of hydrogen and oxygen, the FC system produces the dc output voltage.

According to the basic electrochemical relationship between the hydrogen flow and the FC system current, the fuel cell current is given by Eq. (17) [17,19].

$$Ifc = \frac{2FU(10^{-2}) qh_2}{N_0 N_s}; \tag{17}$$

Thus, combining Eqs. (16) and (17), the total power output of the fuel cell is given by Eq. (18). Fuel cell power variation with H_2 pressure and H_2 flow rate is given in Figs. 12 and 13. The fuel cell model generates 5 kW power at maximum boundary condition (83 psig H_2 pressure and 7.3 l min^{-1} or 0.0073 m^3 min^{-1}, H_2 flow rate) shown in Figs. 12 and 13, which matches with the given design specification of fuel cell currently used at test-bed of the USV.

$$Pfc = E \times Ifc; \tag{18}$$

4. Power module optimization

The optimization approach that we have used divides the problem into discrete time domains and prioritizes the natural energy

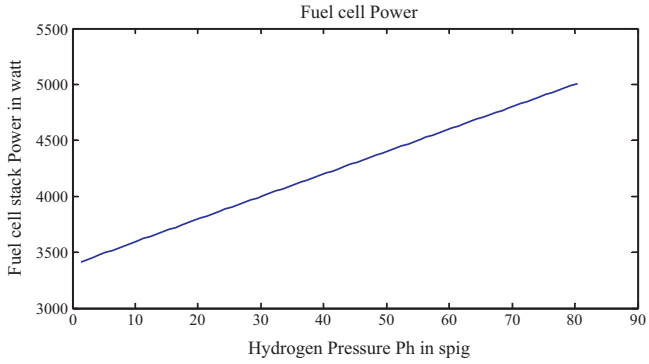

Fig. 12. Fuel cell power with H_2 pressure.

sources over storage energy sources. Solar power remains active during the sun hours of the day normally 8.00 am to 6.00 pm. The wave power generator is used as an alternate to solar power in the night hours and in addition to solar power in day hours whenever wave conditions are favorable.

Both the natural energy sources (solar power and wave power) help to charge the battery bank if supply is more than the demands of the load. If both the power sources are insufficient to meet the demands then the cost optimization module (battery bank, fuel cell system and diesel generator) serves to meet the static and the random power requirement of the load. This optimization module minimizes an error between the demand and supply energy subjected to the priorities of power sources and under the feasible bounds and constraints. The priority definition is based on the consumption cost and on the availability of each source. The diesel generator which is most costly and noisy has lowest priority. The battery bank has higher priority over the fuel cell system since the stored hydrogen fuel is more expensive than the energy stored in the battery. Also, batteries can be recharged with extra sun or wave power unlike the fuel cell which depends on one-time H_2 storage tank capacity. Solar power and wave power are defined as the highest priority sources when they are available. In the present paper we have shown the model only for the first 24 h and chosen to keep it simple in the beginning. In addition, during periods of rain, the hybrid system would operate similar as its operation in night hours (absence of sun). Thus it can be a feasible test condition with the current optimization model. The wave conversion model is limited for an operating range of wave amplitude and angular velocity at 1 m and 0.6π rad s^{-1}.

The energy demands (load profile) vary according to the mission operation and the class of operations within the given type of fleet. In this work, the energy demand is considered for the MS class of USV mission. The objective function to be minimized here is an error between the sum of nonlinear function models of each power source and mission objective. The discrete time optimization is obtained for each single hour separately and in a total period of 24 h. It is a point by point optimization. A pinch point was obtained for an instantaneous value of time "t"(0–23) at each hour separately. This can be extended later to 336 h needed for the ISR mission.

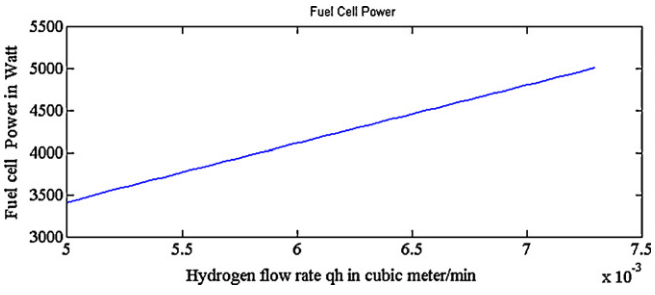

Fig. 13. Fuel cell power with H_2 flow rate (5×10^{-3} to 7.3×10^{-3}) l min^{-1}.

This system design is categorized as a discrete time nonlinear optimization problem with nonlinear constraints. The objective function used is given by Eq. (19)

Objective function:

$$f = (PL + Pm) - (Ps + Pwa + \alpha 3 * Pfc + \alpha 1 * Pb + \alpha 2 * Pd);$$

Minimization of Error= Load profile – Power sources contribution (19)

PL = load profile; P_m = random demand of power by USV; P_s = solar power; P_{wa} = wave power; P_b = battery power; Pfc = fuel cell power; P_d = diesel generator power; $\alpha 1$, $\alpha 2$, $\alpha 3$ = fractional contribution of battery power, diesel generator output and fuel cell power, respectively.

This optimization is subjected to constraints given in Eq. (20) and practically feasible bounds given in Eq. (21)

$$\left.\begin{array}{l}\text{Linear equality}\\ \alpha_2 = 0\\ \text{Linear inequality}\\ \alpha 1 > 0\\ \alpha 3 > 0\\ \text{Nonlinear equality constraints}\\ f = 0\\ \alpha_2 P_d = 0\\ \text{Nonlinear inequality constraints}\\ \alpha 1 P_b > \alpha 2\, P_d\\ \alpha 1 P_b > \alpha 3\, Pfc\\ \alpha 3 Pfc > \alpha 2\, P_d\end{array}\right\} \quad (20)$$

$$\left.\begin{array}{l}0 < \text{battery discharge current in A} < 10\\ 0 < \text{battery discharge time in h} < 5\\ 2 < \text{diesel consumption in G/h} < 160\\ 1.4 < H_2 \text{ pressure in psig} < 82\\ 0.005 < H_2 \text{ flow rate cubic in l min}^{-1} < 0.0073\\ 0 < \alpha 1 < 1\\ 0 < \alpha 2 < 1\\ 0 < \alpha 3 < 1\\ 0 < \text{no. of solar panels in use} < 15\end{array}\right\} \quad (21)$$

4.1. Optimization results

The discrete time optimization for each hour is achieved using Constraints nonlinear minimization (Fmincon) solver with interior point algorithm in the Optimization toolbox in Matlab [20]. The interior-point approach is a method to solve a sequence of approximate minimization problems using the Quasi-Newton line-search method. Nine control variables are used in the problem to achieve the optimized results. A local minimum is found in every discrete hour separately that satisfies the constraints. Optimization is completed because the objective function is a non-decreasing in feasible directions, and constraints were satisfied within the default value of the constraint tolerance. Solar power and wave power models are not included in the optimization since both sources should be used at their maximum capacity on their availability. Therefore,

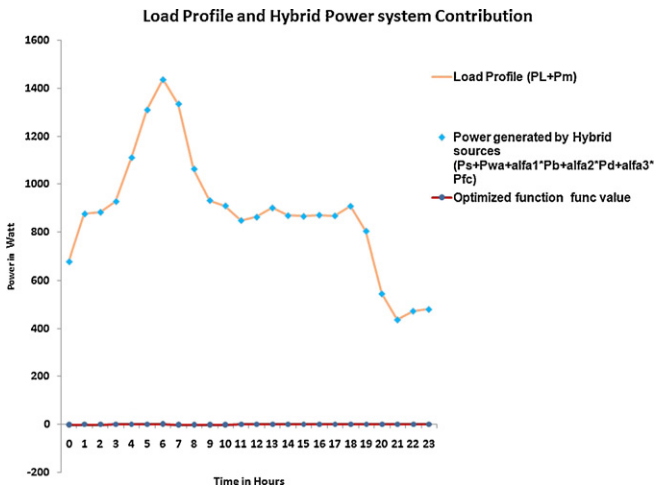

Fig. 14. Load profile and optimized hybrid power system response.

both the source models do not have any variables to be optimized except the number of solar panels in use (see Eq. (21)). This would leave the excess energy from the extra solar panels to charge the battery bank.

The optimized hybrid power system response is shown in Fig. 14 which exactly follows the load profile (mission objectives) at each hour during operation. Fig. 14 also shows the final value of objective function $f = 0$ which is an error between the load profile and hybrid power system response.

Fig. 15 clearly shows the individual contribution of each source to meet the load profile where diesel generator contribution is almost zero. Wave power linear generator contribution is close to 48 W constant power for constant wave frequency at 1 Hz and amplitude of 1 m. Solar power contributes most during the day hours and forces the battery bank and the fuel cell contributions to their lowest. In the remaining hours of operation, the battery bank (considering 5 parallel strings of 4 series batteries each of 3.7 V for this study with maximum discharge current of 10 Amp and maximum voltage is approximately 12 V, Thus total maximum power available to the system is $5 \times 10 \times 12 = 600$ W) contributes over and above to the fuel cell contribution except in the 6th and 7th hours where fuel cell contributes on average 11% more than the battery bank to meet the load profile. In Fig. 16, it is obvious that the battery bank was exhausted to its maximum limit for the said hours.

Fig. 17 shows percentage contribution of each source of the hybrid power system to meet the load profile. Diesel generator's 0% contribution is as assumed. Wave power contributes as low as 5.5% that mostly depends on the efficiency of the linear generator

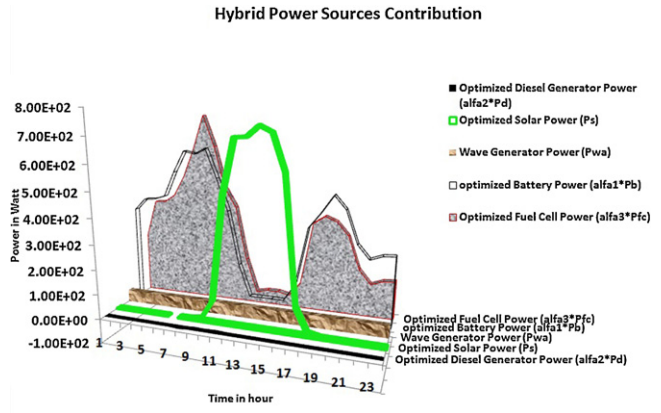

Fig. 15. Hybrid power sources contribution to meet load profile.

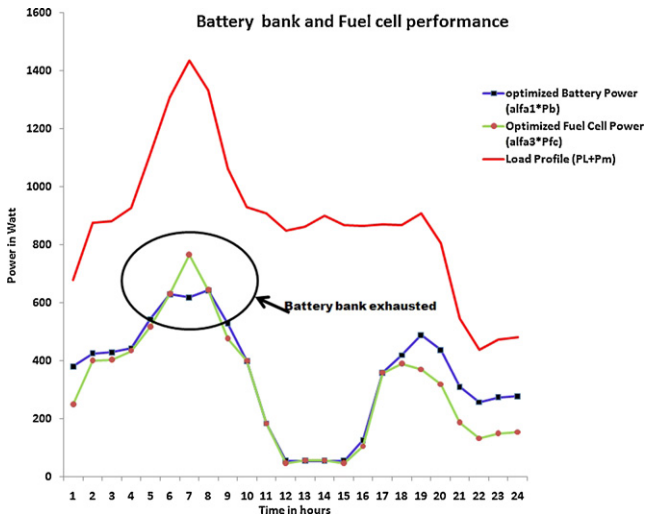

Fig. 16. Battery bank and fuel cell performance.

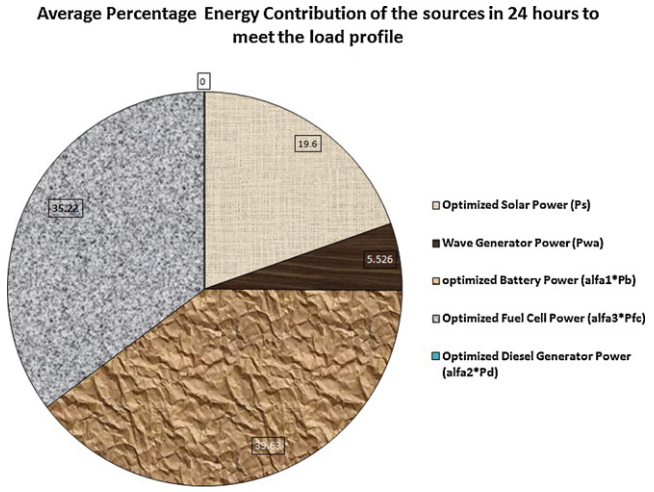

Fig. 17. Average percentage contribution of each hybrid source.

and weather conditions. We have assumed some constant favorable weather conditions for the wave harvester (linear generator) in this study. The battery bank contribution is 39.63% which is 4.41% more than the fuel cell. The solar array shares 19.6% power

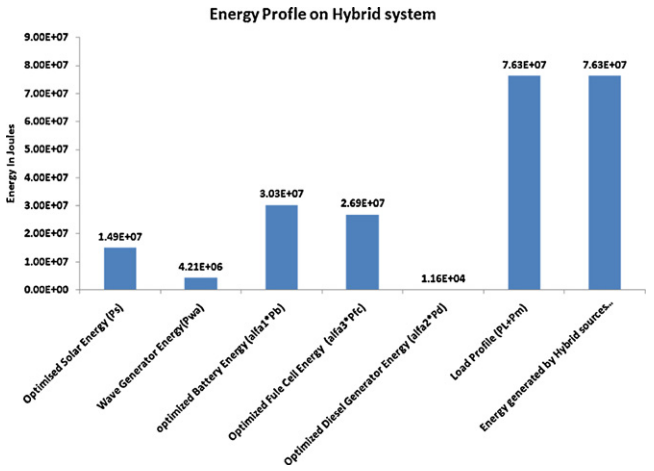

Fig. 18. Energy profile of hybrid system over 24 h.

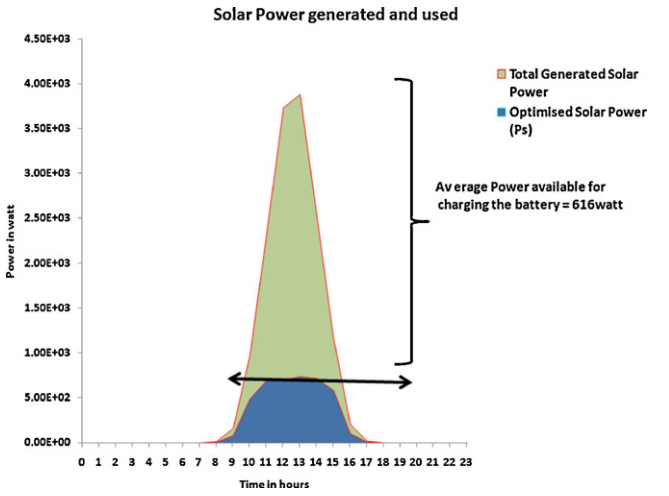

Fig. 19. Solar power generated and used.

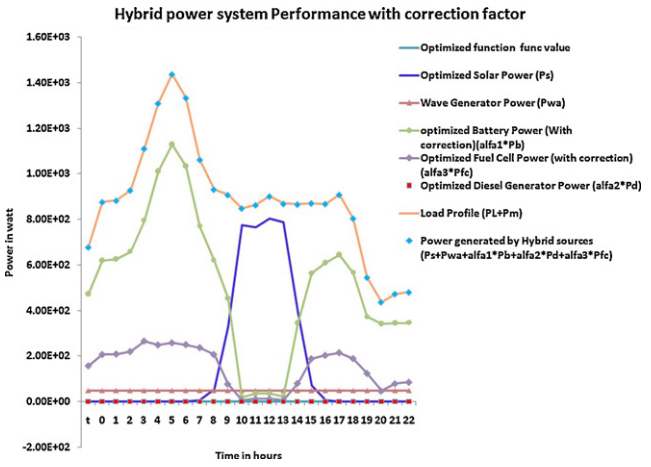

Fig. 20. Hybrid power system performance after correction.

to match to load demand with 15 panels on board considering 700–1000 W m^{-2} solar intensity range during day hours.

Fig. 18 shows an energy profile of each element of the hybrid power system over the 24 h period. This chart helps to resize power system components in the system design during the operation and offline. The total energy required by the USV and supplied through hybrid sources is 7.63×0^7 J. The fuel cell capacity is required to deliver 2.69×10^7 J. This would need a H_2 storage tank capacity of approximately 10 l compared to an existing proposed capacity of 60 l H_2 storage available for a single day's consumption [1].

We have assumed 5 strings of batteries in the bank with 12 V 60 A h Li-ion battery that generates total 1.29×10^7 J ($5 \times 12 \times 60 \times 3600$) energy. The available energy of the battery bank is approximately half the amount of the optimized system requirement (3.03×10^7 J). Hence, the required battery capacity is 701 A h ($3.03 \times 10^7/3600 \times 12$). To make-up this gap, we doubled the battery bank size in the second case optimization. The battery bank size we have decided to begin with is 5 parallel strings of 4 series of batteries (5×4) each of 3.7 V and 60 A h. The Available capacity with the 5×4 battery bank is 300 A h which is equal to 5×60 A h. Making battery bank size double, 10 parallel strings of 4 series of batteries, (10×4) the available capacity becomes 600 A h equal to 10×60 A h.

The required solar energy in the optimized hybrid power system is less than the energy available from 15 panels each with a maximum power output of 200 W but only an average of 41 W during 10 h of sun. The average available energy from the solar array is ($15 \times 41 \times 10 \times 3600$) = 2.21×10^7 J that is 48.3% higher than the required for the load demands during the day light hours. This extra solar energy (0.72×10^7 J or 166.6 A h) is available to recharge the battery bank every day in favorable weather conditions see Fig. 19.

Therefore,

Total battery capacity needed for 24 h = 701 A h.
The available battery capacity in the battery bank (10×4) = 600 A h.
Recharge capacity from sun = 166 A h.

The sum of the available capacity in the battery bank (600 A h) and recharge capacity from the sun (166 A h) is equal to 766 A h. The 766 A h is more than the required battery capacity (701 A h) for 24 h.

According to our study, even with the worst case scenario (the absence of solar power to recharge the battery bank), we would need a battery bank size that can provide capacity higher than 701 A h for 24 h. The battery bank size 12×4 will provide $12 \times 60 = 720$ A h to carry the load demand for 24 h without any recharging.

Now we can see,

Total battery capacity needed for 14 days = $701 \times 14 = 9814$ A h.
Worst case, available capacity in battery bank for 14 days = $720 \times 14 = 10080$ A h.
Obviously, the battery bank size needed to provide 10,080 A h is $14 \times 12 \times 4 = 672$ batteries.

In the previous studies [15], the estimated battery bank size is given as 48×48 totaling 2304 batteries for USV. Therefore, the recommended battery bank size from our study is much less than the already available battery bank size.

In the present paper, we have included a battery bank size for 24 h not for 336 h. A careful analysis of layout design of USV would be needed for appropriate size of battery bank for 336 h. We will include it in subsequent work.

A second optimization case study is achieved with correction applied in battery bank size and with an additional constraint which made the battery bank contribution at least three times higher than the fuel cell contribution as shown in Eq. (23).

$$\alpha_1 \times P_b \geq 3 \times \alpha_3 \times Pfc \tag{23}$$

Fig. 20 shows optimized hybrid power system response for the second case optimization and the performance of each of its elements.

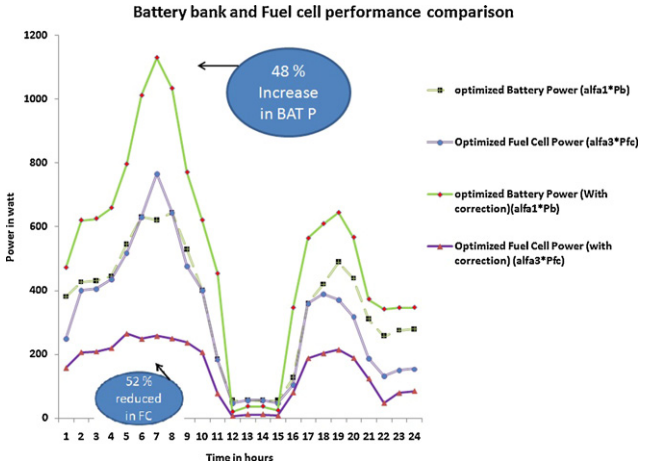

Fig. 21. Battery bank and fuel cell performance.

A local minimum has been found for each hour of discrete time optimization. Hybrid power system response follows the load profile demand with the error as low as −4.28E−09.

The fuel cell performance above the battery bank performance in Fig. 16, violates the constraint. However, Fig. 20 shows the battery bank contribution is around three times higher than the fuel cell contribution. The result maintains the constraints. When the solar array contributes its maximum to the system during the day hours, the battery and fuel cell participate at their minimum level. Diesel generator does not contribute to the system during this stealth operation.

Fig. 21 gives a close look of the battery bank and the fuel cell stack performances during the two cases of optimization. In the first case of optimization the battery bank performance and the fuel cell performance follow almost similar patterns with a slightly larger share for the battery bank. The pattern also breaks the constraints $\alpha 1\, P_b > \alpha 3\, Pfc$ at 6th and 7th hours of operation when the fuel cell performs above the battery bank. To correct the patterns, we applied corrections in the constraints and to the battery bank size. The marked patterns are the corrected patterns which satisfy all constraints and could confirm the higher priority of the battery bank than the expensive fuel cell system. Battery bank contribution has increased by an average of 48.5% and fuel cell share has been reduced by 52% compared to the first case of optimization.

5. Conclusions

This paper presents a unique method to optimize a hybrid power system to meet the power demand of a USV for 24 h. The results can be extended to cover the 336 h required for the MS mission. The mix of hybrid power can support the dynamic and unpredictable demands of the USV. The optimization results are used in resizing the hybrid system design that will eventually establish a compromise between weight and propulsion drag. The prioritization of sources based on their availability and cost optimization prevent a system from being over sized or under sized at crucial demand of load at any discrete time of operation. The natural energy sources (solar array and wave energy converter) are used up to their maximum limits and are also used to charge the battery bank to facilitate long duration ISR operation of the USV. Already defined, feasible constraints on system control variables help to provide better control over variables of each power source. Additionally, optimized system control variables make the system remain stable in any discrete hour. This study limits the diesel fuel consumption to zero except when transiting back and forth to the mother ship. The study may be extended to achieve a globally optimum solution for any USV.

Acknowledgement

This project was supported by a grant from the Office of Naval Research (Contract No. N00024-07-C-4212).

References

[1] N.H. Narayan, P. Singh, Proceedings of the 23rd EVS, The 23rd International Battery, Hybrid and Fuel Cell Electric Vehicle Symposium and Exposition, December, 2007.
[2] T.M. Ramachandrudu, P. Singh, Proceedings of the 25th EVS Conference Sustainable Mobility Revolution, China, November, 2010.
[3] M. Knauff, J. McLaughlin, C. Dafis, D. Niebur, P. Singh, H. Kwatny, C. Nwankpa, Intelligent Ship Symposium, May, 2007.
[4] M. Uzunoglu, O.C. Onar, M.S. Alam, Renewable Energy 34 (June) (2009) 509–520.
[5] A. Hajizadeh, M.A. Golkar, Electrical Power and Energy Systems 29 (2007) 783–795.
[6] K.-S. Jeong, W.Y. Lee, C.S. Kim, Journal of Power Sources 145 (2005) 319–326.
[7] S.J. Moura, H.K. Fathy, D.S. Claway, J.L. Stein, Control Systems Technology, IEEE Transactions 99 (March) (2010) 1–11.
[8] E. Fabrizio, V. Corrado, M. Filippi, Renewable Energy 35 (March) (2010) 644–655.
[9] A.J. del Real, A. Arce, C. Bordons, Journal of Power Sources 193 (2009) 315–321.
[10] The Navy Unmanned Surface Vehicle Master Plan, Department of the Navy, USA, July 2007.
[11] Gilbert Masters, Renewable and Efficient Electrical Power System, John Wiley & Sons Inc. Publication, 2004.
[12] National Solar Radiation Database, User manual, Technical Report NREL/TP-581-41364, April 2007.
[13] C. Ghita, Chirila, A.I. Chirila, I.D. Deaconu, V. Navrapescu, D.I. Ilina, Electrotechnical Conference (2008) 640–645.
[14] I.A. Ivanova, O. Agren, H. Bernhoff, M. Leijon, Underwater Technology (2004) 345–348.
[15] K. Schmieder, Optimization of a fuel cell, electrolyzer and hydrogen storage unit for a hybrid unmanned surface vehicle, MS Thesis, Villanova University, July 2009.
[16] www.dieselserviceandsupply.com.
[17] M.Y. El-Shark, A. Rahman, M.S. Alam, P.C. Byrne, A.A. Sakla, T.A. Thomas, Journal of Power Sources 138 (2004) 199–204.
[18] J. Hamelin, K. Agbossou, A. Laperriere, F. Laurencelle, T.K. Bose, International Journal of Hydrogen Energy 26 (6) (2001) 625–629.
[19] K.H. Hauer, Analysis tool for fuel cell vehicle hardware and software (controls) with an application to fuel cell economy comparisons of alternative system designs, Ph.D. Dissertation, Department of Transportation Technology and Policy, University of California Davis, 2001.
[20] P. Venkataraman, Applied Optimization with MATLAB Programming, John Wiley & Sons Inc. Publication, 2009.